Gas Sensitivity of $In_{0.3}Ga_{0.7}As$ Surface QDs Coupled to Multilayer Buried QDs

Guodong WANG[1*], Zengguang LIU[1], Junjun WANG[1], Yingli YANG[2], Xiaolian LIU[1], Xinran ZHANG[1], Liwei ZHANG[1], and Guohua CAO[1]

[1]*School of Physics and Electronic Information Engineering, Henan Polytechnic University, Jiaozuo 454000, China*

[2]*College of Computer Science and Technology, Henan Polytechnic University, Jiaozuo 454000, China*

*Corresponding author: Guodong WANG   E-mail: wgdhpu@hotmail.com

Abstract: A detailed analysis of the electrical response of $In_{0.3}Ga_{0.7}As$ surface quantum dots (SQDs) coupled to 5-layer buried quantum dots (BQDs) is carried out as a function of ethanol and acetone concentration while temperature-dependent photoluminescence (PL) spectra are also analyzed. The coupling structure is grown by solid source molecular beam epitaxy. Carrier transport from BQDs to SQDs is confirmed by the temperature-dependent PL spectra. The importance of the surface states for the sensing application is once more highlighted. The results show that not only the exposure to the target gas but also the illumination affect the electrical response of the coupling sample strongly. In the ethanol atmosphere and under the illumination, the sheet resistance of the coupling structure decays by 50% while it remains nearly constant for the reference structure with only the 5-layer BQDs but not the SQDs. The strong dependence of the electrical response on the gas concentration makes SQDs very suitable for the development of integrated micrometer-sized gas sensor devices.

Keywords: Surface quantum dots; InGaAs; gas sensitivity

1. Introduction

In recent years, the presence of hazardous chemicals, urban environmental pollutants, and dangerous pollutants in food has promoted the development of high-sensitivity sensors and new sensing materials [1–4]. Semiconductor nanomaterials are ideal gas sensing materials due to their unique small size effect, surface effect, and quantum effect. III-V semiconductor quantum dots (InAs, InGaAs, InP, etc.) formed in self-organized growth mode are typical nanomaterials, widely used in optoelectronic fields like laser, photodetector, LED, and solar cell [5–9]. Lately, InGaAs (InP)

surface quantum dots (SQDs) have also attracted much attention in the application field of gas sensing materials [10–12]. Optical properties of coupling structure with the SQDs stacking on multilayer buried quantum dots (BQDs) have been studied in depth [13–15]. In such coupling structures, carriers transferred from BQDs to SQDs have important influence to enhance photoluminescence (PL) efficiency. Lin *et al*.[16] found that both SQDs and BQDs are sensitive to surface passivation in a coupling structure consisting of a layer of InAs SQDs stacking on two layers of InAs BQDs. The results show that the multi-layer coupled quantum dots structure is very sensitive to the surface

environment and therefore a very suitable gas sensing material. However, very few studies have been reported regarding the impact of external conditions on the electrical properties of SQDs coupled to multi-layer BQDs. A significant sensitivity of the coupling structure to a target gas would be necessary towards device applications.

In this work, the samples were grown by molecular beam epitaxy (MBE) and electrodes were evaporated on the surface by magnetron sputtering. Sheet resistance of the samples dependent on the ethanol and acetone concentration was studied carefully, which provides ideas for the research of highly integrated gas sensors.

2. Experiments

The multi-layer coupling sample was grown in a solid source MBE reactor on semi-insulating GaAs (001) substrates. The schematic diagram of the coupling structure is shown in Fig. 1(a). The temperature mentioned below by describing the MBE growth condition refers to the substrate temperature. Firstly, after thermally removing the native oxide layer from the GaAs substrate at $600\,^\circ\mathrm{C}$, a 150 nm GaAs buffer layer, a 200 nm $Al_{0.3}Ga_{0.7}As$ etch stop layer, a 200 nm Si doped layer (at a doping concentration of $1\times10^{18}\,\mathrm{cm}^{-3}$), and a 40 nm un-doped GaAs layer were deposited at $580\,^\circ\mathrm{C}$ in sequence. Then, 11 monolayers (ML) of $In_{0.3}Ga_{0.7}As$ were grown at $505\,^\circ\mathrm{C}$ to form a layer of BQDs capped with 10 nm GaAs. The BQD layer and the GaAs capping layer were repeated five times. Finally, 11 MLs of $In_{0.3}Ga_{0.7}As$ were deposited to form the SQDs on the top of the sample without the GaAs capping layer. For comparison, a reference sample, with all the other layers the same and the absence of the top $In_{0.3}Ga_{0.7}As$ SQDs, was also grown and characterized. The formation of both SQDs and BQDs was confirmed by the transition of the in-situ reflection-high-energy-electron-diffraction pattern from streaky to spotty. For PL measurements, the samples were mounted on the cold finger of a
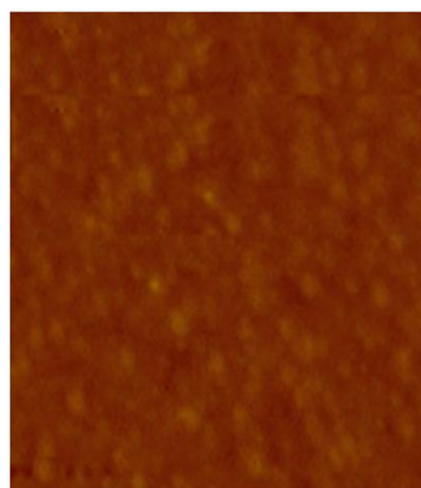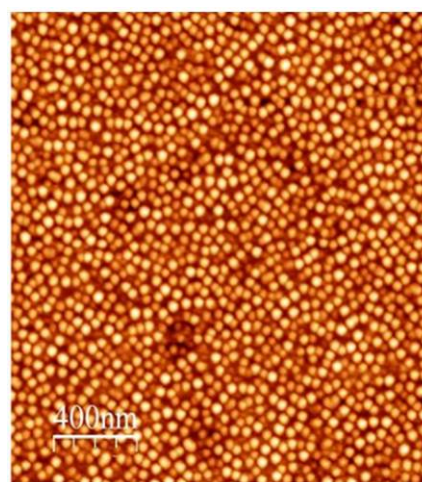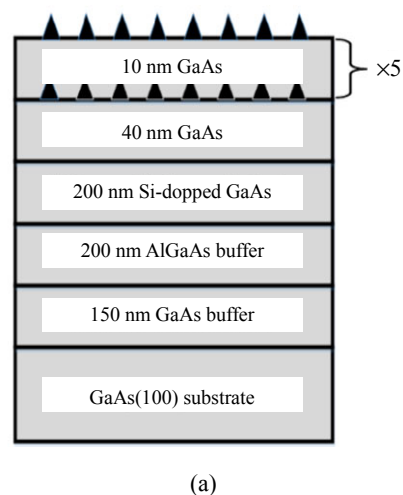

(a)

(b)

(c)

Fig. 1 Schematic diagram and atomic force microscope (AFM) image of the SQDs: (a) schematic diagram of the stacking SQDs structure, (b) 2 μm × 2 μm AFM image of the SQDs, and (c) 2 μm ×2 μm AFM image of the reference sample surface.

closed-cycle cryostat with temperature varying between 10 K and 300 K. An excitation laser, with an emission wavelength of 532 nm, was focused on the sample surface to a spot diameter of a few micrometers by a 50× objective lens. The PL signal was dispersed by an Acton-50 cm spectrometer and then detected by a liquid-nitrogen cooled charge coupled device detector array. The purpose of depositing the etch stop layer and Si doped GaAs layer is to facilitate the fabrication of sensor electrodes in the future work.

Electrode 2500 μm×2500 μm

2000 μm

(a)

LED

Multimeter

Vacuum chamber
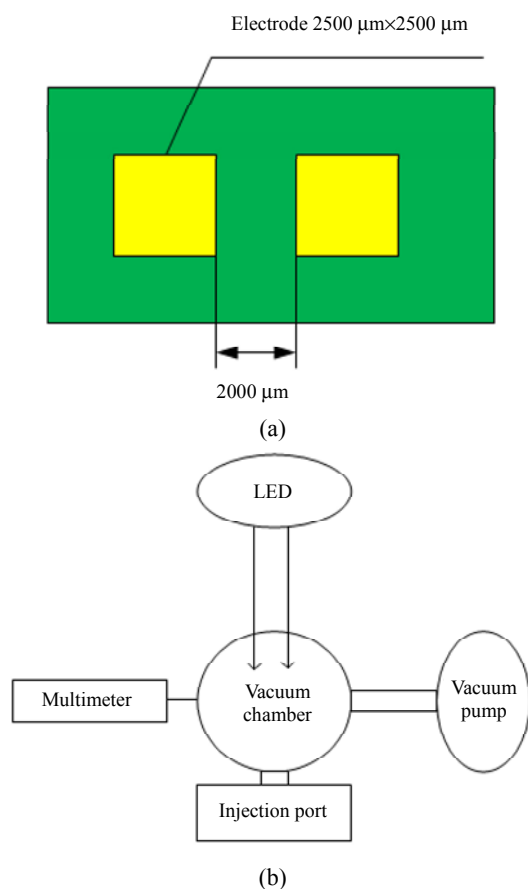
Vacuum pump

Injection port

(b)

Fig. 2 Schematic diagram of the electrode pattern and gas-sensing test system: (a) electrode pattern and (b) gas-sensing test system.

In order to measure the gas sensing properties of the samples, a pair of metal electrodes were sputtered on the surface of the samples by magnetron sputtering. The size of the electrodes was 2.5×2.5 mm^2 separated by 2 mm, as shown in Fig. 2(a). The gas sensing measurement was carried out on a self-built test platform, which consisted of a

vacuum test chamber, a vacuum pump, a digital multimeter, and an LED light source, as shown in Fig. 2(b). Ethanol and acetone gases used in the experiments were obtained by placing 100 mL ethanol and acetone liquid in a sealed reagent bottle with a volume of 500 ml, respectively. At room temperature, the saturated gas was formed by the natural volatilization of ethanol and acetone. The ethanol or acetone gas was extracted quantitatively from the reagent bottle by a syringe and injected into the vacuum test chamber. After the gas was fully diffused, the sheet resistance of the samples was measured.

3. Results and discussion

Figure 1(b) shows the 2 μm ×2 μm AFM image of the SQDs with the dot density estimated to be 3.8×10^{10} cm^{-2}, the average height (6.9±1.3) nm and the average diameter (46±6) nm. No defects or large overlapped islands were observed on the surface of the sample, indicating good QD quality. For comparison, the AFM image of the surface of the reference sample is illustrated in Fig. 1(c). It is obvious that the surface of the reference sample is smooth due to the absence of the SQDs.

The PL spectra were measured at 70 K with a laser excitation intensity of 10 W/cm^2 for both the coupling sample and the reference one. As plotted in Fig. 3, there is a significant difference between the PL spectra of these two samples. The reference sample shows a perfect Gaussian PL signal centered at 1188 meV with a linewidth of 53.48 meV, which can be attributed to the fundamental electronic transition in the five layers of BQDs [17]. However, the PL spectrum of the coupling structure has two prominent PL peaks. One is centered at 1182 meV with a linewidth of 51.36 meV. In consideration of the PL emission from the BQDs of the reference sample, this peak is attributed to the emission from BQDs. The other peak, centered at 942 meV with a linewidth of 103.81 meV, is attributed to the emission from the SQDs. The SQD peak is

redshifted with respect to that of the BQDs by about 240 meV, because the SQDs are not strained by a capping layer and their lattice constant and thus the band gap approaches the natural values [15, 17].
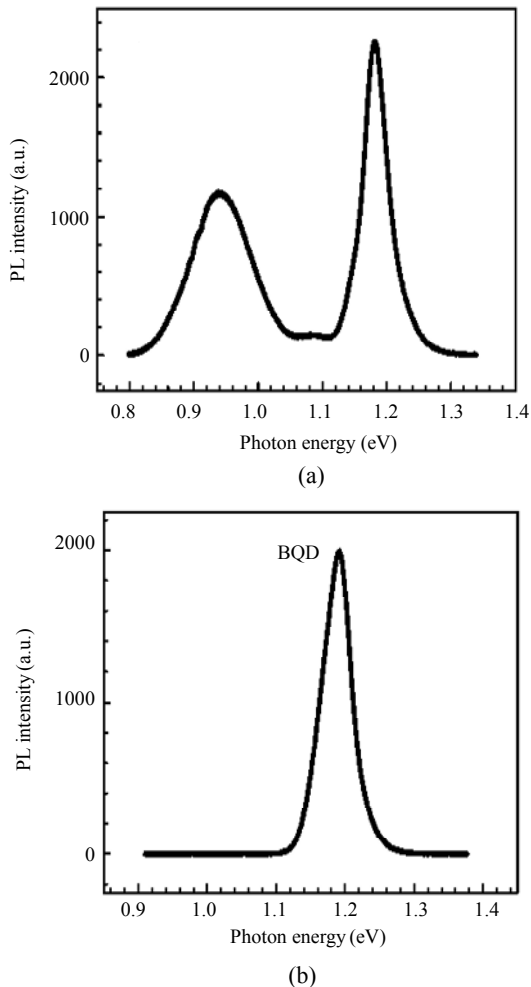

(a)

(b)

Fig. 3 PL spectra measured at T=70 K: (a) PL spectrum of the coupling sample and (b) PL spectrum of the reference sample.

As we know, due to the carriers transferred from BQDs to SQDs, the PL intensity of the SQDs increases obviously. However, when the number of the BQDs layers exceeds five, the enhancement of the PL intensity of the SQDs will slow down. Moreover, the more the BQDs layers are, the more complex the sample deposition process is and the higher the cost is. As a compromise, we set the number of the BQDs layers as five.

The thickness of the GaAs isolation layer is only 10 nm. The photo-excited carriers in the BQDs layer can be easily coupled to the SQDs layer, in other words, there is a strong coupling between the SQDs layer and the BQDs layer [18]. We plotted the integrated intensity of the PL spectra of the coupling structure and the reference one dependent on the temperature in Fig. 4. For convenience, the integrated PL intensity is normalized. The curve of the former has a different tendency as compared with that of the latter. The integrated PL intensity of the reference sample remains almost constant at low temperatures, beginning to decrease significantly when the temperature is higher than 200 K and at 300 K, and drop to only 0.17% of that at 10 K. This can be explained as follows. In the BQDs, the thermal activation energy differs from dot to dot due to the size distribution. As the temperature increases, excitons at smaller dots can easily be thermally activated to overcome the energy barrier produced by the wetting layer, and then recapture into the larger size dots. In this process, there is ideally no net loss of carriers from the BQDs. As a result, the integrated PL intensity of the BQDs keeps almost constant in the temperature range of 10 K−200 K. when the temperature increases further, phonon scattering starts to dominate and nonradiative recombination of the excitons increases resulting in a rapid decline of the integrated PL intensity of the BQDs from 200 K up to room temperature.

Similarly, there is also thermal activation and recapture among the BQDs in the coupling structure. However, there is additional transition of photo-generated carriers from BQDs to SQDs in the coupling structure. The photo-generated carriers in the BQDs tend to transfer to the surface layer rather than recombine locally radiatively, leading to an increase in the carrier number in the SQDs. Consequently, the integrated PL intensity of the SQDs decreases slowly with an increasing temperature, while that of the BQDs decreases faster. As seen in Fig. 4, the integrated PL intensity of the SQDs in the coupling structure stays almost constant at low temperatures and begins to decrease significantly at 130 K with the increasing temperature. At 300 K, it decreases to 0.7% of that at

10 K. However, the integrated PL intensity of the BQDs in the coupling structure begins to decrease at 60 K, and it reduces to 0.06% of that at 10 K when the temperature rises to 300 K.
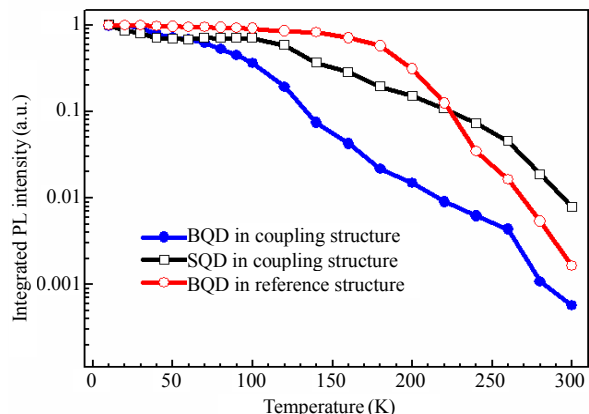

Fig. 4 Integrated PL intensity of two samples as a function of temperature.

An electrical analysis as a function of the incident light and ethanol concentration was performed for both the coupling and reference samples, as shown in Fig. 5. All the tests were carried out at 24℃. A low power white LED was used as the light source to reduce the thermal effect. As shown in Figs. 5(a) and 5(b), when the ethanol concentration increases without illumination, the sheet resistance of the coupling and the reference sample shows almost no change. When the sample is irradiated by the white LED, the sheet resistance of the reference sample is almost constant with an increasing ethanol concentration. However, the sheet resistance of the coupling sample decreases significantly with an increasing ethanol concentration. Therefore, illumination and ethanol gas are two necessary factors for the sheet resistance change of the coupling sample. The reasons can be explained as follows. For the coupling sample, under white light irradiation, a certain number of photo-generated carriers are generated in the BQDs layer and the GaAs layer under the SQDs layer, some of which can be coupled to the SQDs layer. However, these transferred carriers will be captured by surface states in the SQDs and non-radiative recombination will occur. When the ethanol gas is injected into the vacuum chamber, the dangling

bonds can absorb ethanol molecules, which is helpful for the passivation of the surface states leading to the reduction of the density of the active surface states. Thus, the ability of the surface states to capture carriers is weakened, which allows more photo-generated carriers to move through the surface, resulting in an increase in surface conductivity and a significant decrease in the sheet resistance of the coupling structure. For the reference sample, because there is no SQDs layer and the surface is covered by the GaAs layer, the surface states are missing on the quantum dots. Therefore, the sheet resistance of the reference sample is basically unchanged with the variation of the ethanol concentration even in illumination.
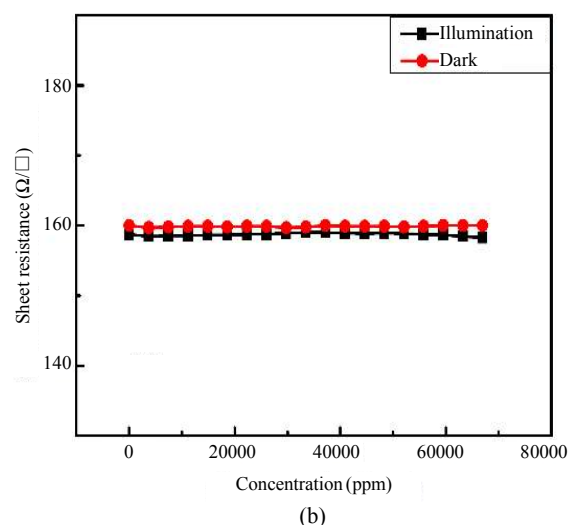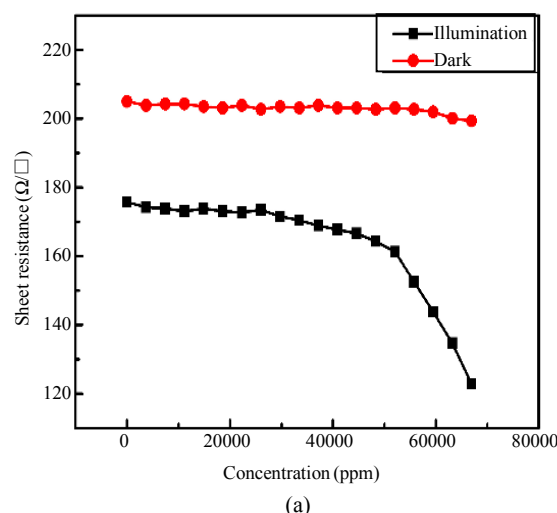

(a)

(b)

Fig. 5 Sheet resistance as a function of the ethanol concentration: (a) the coupling sample and (b) the reference sample.

We notice that there is a big difference in resistance between the coupling and reference samples both in dark and illumination. This is probably caused by two factors. On one side, due to the absence of the SQDs, the metal contact adhesion to the surface of the coupling sample is different from that of the reference sample. On the other side, due to the presence of Si-doped GaAs layer below quantum dots, the carriers in the doped layer are enough and part of them can transfer easily to the surface of both samples due to thermal excitation at room temperature. However, the surface states in the coupling sample will capture most of the carriers from the doped layer, resulting in a higher surface resistance. On the contrary, there are no surface states on quantum dots in the reference sample and consequently the carriers from the doped layer can move freely on the surface of the reference sample, resulting in a lower surface resistance.

The electrical responses of both samples as a function of the acetone concentration are plotted in Fig. 6. By comparing Figs. 6(a) and 6(b), it is found that the sheet resistance of the coupling sample decreases with an increasing acetone concentration in illumination, while that of the reference sample does not change with an increasing acetone concentration regardless illuminated or not. It confirms the importance of the surface morphology of the sample to the gas sensitivity. It can be predicted that samples with a higher density of surface states have even higher sensitivity.

By comparing Figs. 5(a) and 6(a), we found that the sheet resistance of the coupling sample is almost constant in dark. On the contrary, in illumination, the sheet resistance decreases, but the change of the sheet resistance in the ethanol gas is much greater than that in the acetone gas. We can deduce that the SQDs as three-dimensional nanostructures are gas-sensitive, and they show different sensitivities to different kinds of gases. As it is known, ethanol is a polar molecule and acetone is a polar aprotic molecule. With the concentration of the target gas as

60000 ppm, the sheet resistance of the SQD sample changes by 18% in the ethanol gas and 2.5% in the acetone gas. Obviously, acetone has less effect on the sheet resistance than ethanol. We attribute this to different interaction strengths between gas molecules and the surface states. Ethanol has a high dipole moment, so it can interact with the surface states of QDs more easily than acetone. The surface states of QDs are the main obstacles to the surface motion of the photoexcited carriers. Because of the high specific surface area of the QDs structure and a big number of surface eigenstates, the surface resistance is detectable. Therefore, we conclude that the surface conductivity of the SQDs gets higher and the sensitivity of the SQDs gets stronger for gases with stronger polarity than ethanol.
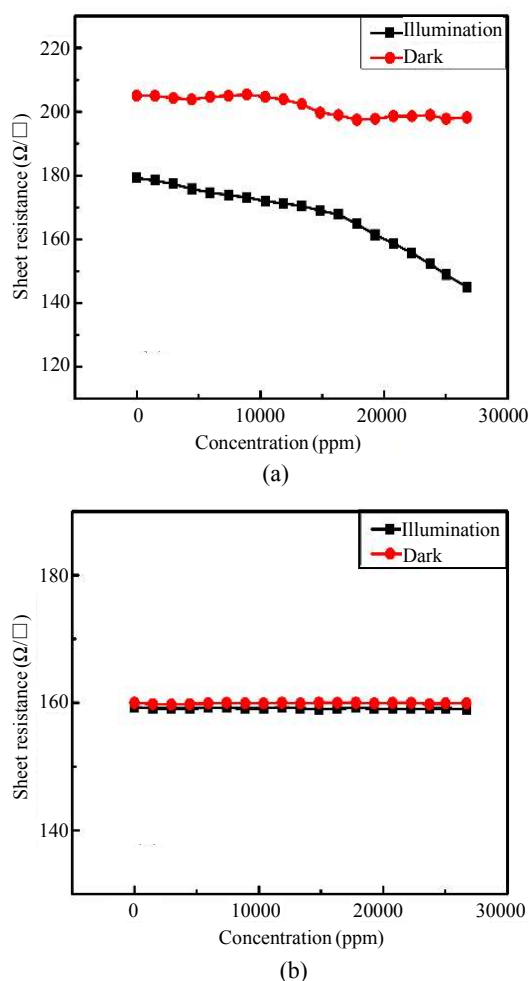

Fig. 6 Sheet resistance as a function of the acetone concentration: (a) the coupling sample and (b) the reference sample.

From Figs. 5(a) and 6(a), we also find that the coupling sample has a steeper slope in the response curve both for ethanol and acetone when the gas concentration is higher than 50000 ppm. This indicates that the sample is more suitable for the detection of high concentration gases.

In order to analyze the selectivity of the samples, Fig. 7 shows the response of the coupling sample for both ethanol and acetone in the high concentration range. It can be seen that the change rates of the resistance for both samples are quite different at the same concentration of the ethanol and acetone gas. In the ethanol gas (70000 ppm), the change rate of the resistance is relatively large (30%), while in the acetone gas (70000 ppm), the change rate is very small (3%). It shows that the coupling sample has higher selectivity for the ethanol gas.
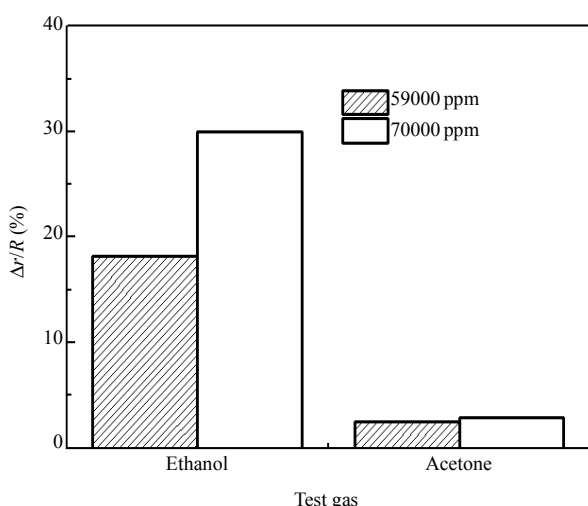

Fig. 7 Response of the coupling sample for different gases.

4. Conclusions

In summary, a sample with In$_{0.3}$Ga$_{0.7}$As SQDs coupled to multilayer BQDs and a reference sample without the SQDs are grown by MBE for the gas sensitivity investigation. The temperature dependent PL spectra are proved that there is a strong carrier transport from BQDs to SQDs. The electrical response of the In$_{0.3}$Ga$_{0.7}$As SQDs is analyzed as functions of the incident light and gas concentration. The results show that the surface conductivity of the coupling sample is sensitive to acetone and ethanol in illumination. The acetone or ethanol molecules can be absorbed by the surface states resulting in surface passivation. Consequently, the carrier conductivity performance of the sample surface is improved and the surface resistance is reduced. The stronger the polarity of gas molecules is, the greater the influence on the surface resistance of the SQDs is. This work is helpful for the realization of highly integrated gas sensors and has certain guiding significance for the development of integrated micrometer-sized gas sensor devices.

References

[1] S. S. Zhang, G. Sun, Y. W. Li, B. Zhang, L. Lin, Y. Wang, *et al.*, "Continuously improved gas-sensing performance of SnO$_2$/Zn$_2$SnO$_4$ porous cubes by structure evolution and further NiO decoration," *Sensors and Actuators B: Chemical*, 2018, 255: 2936–2943.

[2] T. N. N. Dau, V. H. Vu, T. T. Cao, V. C. Nguyen, C. T. Ly, D. L. Tran, *et al.*, "In-situ electrochemically deposited Fe$_3$O$_4$ nanoparticles onto graphene nanosheets as amperometric amplifier for electrochemical biosensing applications," *Sensors and Actuators B: Chemical*, 2019, 283: 52–60.

[3] R. Alrammouz, J. Podlecki, P. Abboud, B. Sorli, and R. Habchi, "A review on flexible gas sensors: from materials to devices," *Sensors and Actuators A,* 2018, 284: 209–231.

[4] Z. Xiao, L. B. Kong, S. C. Ruan, X. L. Li, S. J. Yu, X. Y. Li, *et al.*, "Recent development in nanocarbon materials for gas sensor applications," *Sensors and Actuators B: Chemical*, 2018, 274: 235.

[5] J. Kwoen, B. Jang, J. Lee, T. Kageyama, K. Watanabe, and Y. Arakawa, "All MBE grown InAs/GaAs quantum dots lasers on on-axis Si (001) ," *Optics Express*, 2018, 26(9): 11568.

[6] Q. Li, Y. Huang, J. Ning, C. Jiang, X. Wang, H. Chen, *et al.*, "InAs/GaAs quantum dot dual-mode distributed feedback laser towards large tuning range continuous-wave terahertz application," *Nanoscale Research Letters*, 2018, 13(1): 267.

[7] D. Kim, S. Hatch, J. Wu, K. A. Sablon, P. Lam, P. Jurczak, *et al.*, "Type-II InAs/GaAsSb quantum dot solar cells with GaAs interlayer," *IEEE Journal of Photovoltaics*, 2018, 8(3): 741.

[8] Y. Bidaux, K. A. Fedorova, D. A. Livshits, E. U. Rafailov, and J. Faist, "Investigation of the chromatic dispersion in two section InAs/GaAs quantum-dot lasers," *IEEE Photonics Technology Letters*, 2017, 29(24): 2246.

[9] N. S. Beattie, P. See, G. Zoppi, P. M. U. M. Duchamp, I. Farrer, D. A. Ritchie, *et al.*, "Quantum engineering of InAs/GaAs quantum dot based intermediate band solar cells," *ACS Photonic*, 2017, 4(11): 2745.

[10] R. D. Angelis, M. Casalboni, L. D. Amico, F. D. Matteis, F. Hatami, W. T. Masselink, *et al.*, "Vapour sensitivity of InP surface quantum dots," *Key Engineering Materials*, 2014, 605: 177.

[11] R. D. Angelis, M. Casalboni, F. D. Matteis, F. Hatami, W. T. Masselink, H. Zhang, *et al.*, "Chemical sensitivity of InP/In$_{0.48}$G$_{a0.52}$P surface quantum dots studied by time-resolved photoluminescence spectroscopy," *Journal of Luminescence*, 2015, 168: 54.

[12] M. J. Milla, J. M. Ulloa, and A. Guzman, "Photoexcited-induced sensitivity of InGaAs surface QDs to environment," *Nanotechnology*, 2014, 25(44): 445501.

[13] B. L. Liang, Z. M. Wang, Y. I. Mazur, and G. J. Salamo, "Photoluminescence of surface InAs quantum dot stacking on multiplayer buried quantum dots," *Applied Physics Letters*, 2006, 89(24): 243124.

[14] Q. Yuan, B. L. Liang, C. Zhou, Y. Wang, Y. N. Guo, S. F. Wang, *et al.*, "Interplay effect of temperature and excitation intensity on the photoluminescence characteristics of InGaAs/GaAs surface quantum dots," *Nanoscale Research Letters*, 2018, 13(1): 387.

[15] B. L. Liang, Z. M. Wang, Y. I. Mazur, S. Seydmohamadi, M. E. Ware, and G. J. Salamo, "Tuning the optical performance of surface quantum dots in InGaAs/GaAs hybrid structures," *Optics Express*, 2007, 15(13): 8157.

[16] A. Lin, B. L. Liang, V. G. Dorogan, Yu I. Mazur, G. G. Tarasov, G. J. Salamo, *et al.*, "Strong passivation effects on the properties of an InAs surface quantum dot hybrid structure," *Nanotechnology*, 2013, 24(7): 075701.

[17] G. Wang, B. L. Liang, B. C. Juang, A. Das, M. C Debnath, D. L. Huffaker, *et al.*, "Comparative study of photoluminescence from In$_{0.3}$Ga$_{0.7}$As/GaAs surface and buried quantum dots," *Nanotechnology*, 2016, 27(46): 465701.

[18] B. L. Liang, Z. M. Wang, Y. I. Mazur, and G. J. Salamo, "Correlation between surface and buried InAs quantum dots," *Applied Physics Letters*, 2006, 89(4): 043125.